Proceedings of the 1991 IEEE
International Conference on Robotics and Automation
Sacramento, California - April 1991

A Control-Configured Flexible Arm: Integrated Structure/Control Design

H. Asada J.-H. Park S. Rai

Center for Information-Driven Mechanical Systems
Department of Mechanical Engineering
Massachusetts Institute of Technology

Abstract

An innovative approach to the design of a high-speed flexible robot arm is presented. The structure and shape of arm links that allow for fast, stable endpoint control are obtained by using a finite element method. Mass and stiffness distributions as well as the actuator and sensor locations are determined so that the poles and zeros of the system may exist at desired locations in the s-plane.

First, arm links are modeled as flexible beams, the geometry of which are parametrized by using a finite element method. Coordinates of the finite element model are treated as design parameters to be optimized through dynamic evaluation. Dynamic characteristics, in particular pole-zero locations, are represented in relation to the design parameters, i.e. the shape and structure of the arm mechanism. The highlight of the paper is to formulate the inverse relationship of the pole-zero plot back to the arm structure using a generalized Jacobian method. Based on this formulation, we solve the inverse problem of finding an optimal structure that satisfies desired pole-zero specifications. The resultant design of the flexible arm has unique geometric and structural features achieving a significantly high natural frequency and collocated actuator/sensor dynamics. To demonstrate the new method a prototype arm is designed, built, and tested. It is revealed that the new arm configured by the pole-zero plot has significant advantages over its traditional counterparts, which would not be obtained without use of the integrated structure/control design method.

1 Introduction

The majority of flexible robot arms that have been addressed in literature have a simple structure consisting of beams with uniform mass and stiffness distributions. While the simplified beams allow for analytic modeling and theoretical treatment, the arm construction is unrealistically primitive and its dynamic performance is severely limited. If one tries to compensate for the poor dynamics merely by control, it requires a lot of energy and heavy computation, which would end up with an impractical system and unsatisfactory performance. It is judicious to reconsider the mechanical structure along with the controller in order to improve the arm dynamics. The arm structure does not have to have a uniform cross section so as to be mathematically tractable, but its cross section and the mass and stiffness distributions can be varied by treating them as design parameters in order to improve its dynamic performance.

In this paper, we will explore an integrated approach to the design and control of flexible arms. Here, we attempt to optimize the arm structure along with the control. Our design parameter space will be expanded to an order-of-magnitude larger space having both structural and controller design parameters. It is hoped that the integrated approach will allow us to eliminate undesired characteristics in plant dynamics at the structural design stage and provide an optimal match between the mechanical structure and control.

This integrated structure/control design has been attempted in the field of large space structures. Various methods have been developed in order to evaluate robustness and performance of a whole system [Lim and Junkins, 1989], [Belvin and Park, 1990], [Kosut, et al., 1990]. However, the methods for designing the structure are either still based on trial and error, or applicable to only limited cases; no systematic methods for general use have been developed to determine the details of mechanical structures.

The objectives of this paper are to develop a systematic method for designing mechanical structures that meet dynamic specifications and to apply the new method to the design of a flexible robot arm. A computer aided engineering system is developed, which can find link geometry and structure that exhibit desired dynamic characteristics suitable for control. Using this design system we will increase the arm's natural frequency and eliminate non-minimum phase zeros at the same time. The resultant arm structure will allow for fast, stable control, which could not be accomplished without use of the systematic design method.

2 Problem and Approach

In this paper we deal with a single link flexible arm, as shown in Figure 1. Unlike the traditional arm links that have a uniform cross section, the beam discussed in this paper has a varying cross section along the beam axis. As a result, the mass per unit length and the stiffness of each section vary along the arm link. It is our goal to determine an optimal shape of the beam and optimal mass and stiffness distributions on the basis of dynamics evaluation. Namely, the geometry as well as mass and stiffness properties are the design parameters that we wish to optimize.

To describe the beam geometry as well as to evaluate the link dynamics, we use a finite element method [Bathe, 1982]. Analytical models are not applicable to this type of beam where the cross section varies continuously along the beam axis. The finite element method allows us to represent a com-

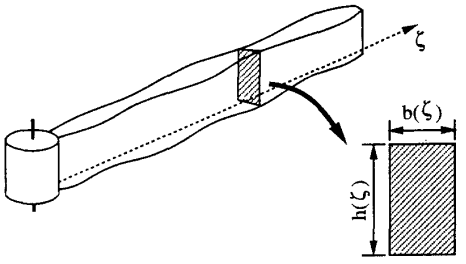

Figure 1: Single link arm with a varying cross section

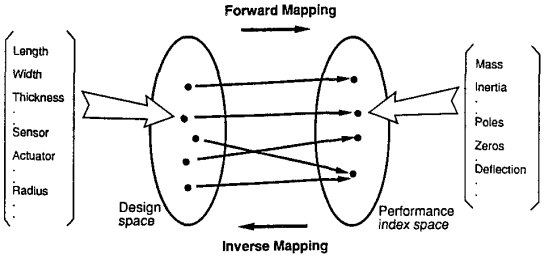

Figure 2: Mapping between design space and performance index space

plicated beam geometry with a varying cross section. Using a sufficient number of elements, the finite element model can represent a continuous system with a desired accuracy.

In the finite element method, geometry is described by coordinates of each knot or control point that constitutes an individual element. In this paper, we treat these coordinates as design variables. Let x_1 through x_n be the design parameter vector given by

$$\mathbf{x} = (x_1, x_2, \cdots, x_n)^T \in R^n \qquad (1)$$

The design parameter vector may include not only geometric parameters but also non-geometric ones. For instance, we can include parameters associated with the locations of actuators and sensors, which have a direct influence upon the system dynamics. The above design parameters can represent a variety of link geometry, but the dimension of the design parameter space tends to be too large. It is desired to reduce the number of design parameters by restricting the shape of the individual elements of the beam structure. For instance, if the cross section of the beam is assumed to be a rectangular, its shape can be represented by two parameters; width and height as shown in Figure 1. In the following design of beam structure we deal with only the rectangular cross section.

In designing a controller, one needs to know the dynamic characteristics of the arm link. In this paper, we use a pole-zero plot for representing the arm dynamics and designing control. To this end, let us describe the locations of poles and zeros relevant to control performance by a set of variables given by

$$\mathbf{p} = (p_1, p_2, \cdots, p_m)^T \in R^m \qquad (2)$$

The vector $\mathbf{p}$ represents dynamic performance indices. The pole-zero locations are dependent upon the geometry of the arm link and the other design parameters. As shown in Figure 2, there is a mapping from the design parameter space to the performance index space. Let us describe the relationship between the design variables $\mathbf{x}$ and the resultant performance indices $\mathbf{p}$ by nonlinear functions;

$$p_i = f_i(x_1, x_2, \cdots, x_n), \qquad 1 \le i \le m \qquad (3)$$

As mentioned previously, we wish to relocate poles and zeros by modifying the structure of the arm as well as by feedback control. Namely, what we would like to do is to find appropriate structure and geometry that relocate poles and zeros to desired locations. To this end, we will solve the inverse problem of the above relationships. Namely, the problem is to determine the arm geometry and other design parameters so that the resultant plant dynamics may have its poles and zeros at specified locations. As shown in Figure 2, this is an inverse mapping from the performance index space back to the design parameter space. As we change the desired pole-zero plot, the corresponding shape and structure of the arm link vary. This inverse mapping will allow the designer to obtain a significant improvement that would not be achieved merely by control. When the pole-zero plot of the original mechanical structure results in an unsatisfactory control performance, the designer can modify the pole-zero configuration by modifying the arm link, which allows for further improvement of control performance. For instance, when the open-loop poles are far from the desired locations, a large feedback gain and large control efforts are required for the system. It is particularly efficient in this case to relocate undesirable poles as well as zeros by modifying the mechanical structure so that the desired control performance can be achieved in an effective way.

The inverse mapping from a pole-zero plot back to the arm-link geometry and structure is highly nonlinear and complex. Generally, solutions to the nonlinear simultaneous equations given by eq. (3) are not unique, or more importantly, might not exist in a certain range of feasible values. Specifically, to obtain a feasible design, changes in the design variables $\mathbf{x}$ must meet some constraints and specifications. For instance, the moment of inertia of the arm link must be lower than a certain limit due to the power limit of the actuator. To meet a load bearing requirement, the static deflection of the arm link must be less than a certain value. Generally, we need to consider a number of specifications and design constraints when solving the inverse problem. Let us formally describe the constraints and specifications by functional relationships given by

$$g_j(x_1, x_2, \cdots, x_n) \le G_j, \qquad 1 \le j \le l \qquad (4)$$

Thus, the inverse problem is to solve eq. (3) for design variables $\mathbf{x}$ subject to the constraints and specifications given by eq. (4), when the pole-zero vector $\mathbf{p}$ is specified. In the following sections, we will solve this problem and derive from the inverse solution a unique arm structure that exhibits a desired control performance. We will take a two-step design procedure. In Section 3, we will focus on the poles of the system and relocate them by modifying the link geometry. In Section 4, we will relocate the zeros by virtually changing the actuator location.

3 Shaping the Arm Link

3.1 Solving the Inverse Problem

As mentioned previously, the relationships between the design variables and the pole-zero locations are highly nonlinear and complex. As we deal with a complicated beam geometry, closed-form analytic functions in the form of eq. (3) cannot be obtained explicitly. In this paper we employ a numerical, iterative method based on sensitivity analysis. Using a Jacobian matrix that represents effects of incremental changes in design variables upon the pole-zero location vector, we will modify the original link geometry incrementally. Let $\mathbf{J}$ be the Jacobian matrix given by

$$\mathbf{J} = \begin{pmatrix} \frac{\partial f_1}{\partial x_1} & \cdots & \frac{\partial f_1}{\partial x_n} \\ \vdots & \ddots & \vdots \\ \frac{\partial f_m}{\partial x_1} & \cdots & \frac{\partial f_m}{\partial x_n} \end{pmatrix} \in R^{m \times n} \tag{5}$$

Incremental changes in design variables $\mathbf{x}$ and performance indices $\mathbf{p}$ are then related by

$$\Delta \mathbf{p} = \mathbf{J} \Delta \mathbf{x} \tag{6}$$

As mentioned in the previous section, the design variables must satisfy the constraints and specifications given by eq. (4). Though the original formulation includes inequality, let us consider the following equality conditions;

$$p_{m+j} = G_j - g_j(x_1, x_2, \cdots, x_n), \qquad 1 \le j \le l \tag{7}$$

where p_j is a non-negative value to be specified in order to satisfy the original conditions. Taking the derivatives of eq. (7) let us incorporate the constraints with the Jacobian matrix;

$$\mathbf{J}_A = \begin{pmatrix} \frac{\partial f_1}{\partial x_1} & \cdots & \frac{\partial f_1}{\partial x_n} \\ \vdots & \ddots & \vdots \\ \frac{\partial f_m}{\partial x_1} & \cdots & \frac{\partial f_m}{\partial x_n} \\ -\frac{\partial g_1}{\partial x_1} & \cdots & -\frac{\partial g_1}{\partial x_n} \\ \vdots & \ddots & \vdots \\ -\frac{\partial g_l}{\partial x_1} & \cdots & -\frac{\partial g_l}{\partial x_n} \end{pmatrix} \in R^{(m+l) \times n} \tag{8}$$

which is referred to as the generalized Jacobian matrix [Baillieul, 1986]. In accordance with the generalized Jacobian, we need to augment vector $\Delta \mathbf{p}$ by adding Δp_{m+j}'s so that

$$\Delta \mathbf{p}_A = [\Delta p_1, \cdots, \Delta p_m, \Delta p_{m+1}, \cdots, \Delta p_{m+l}]^T \in R^{m+l} \tag{9}$$

Now the problem is to solve the linear equation

$$\Delta \mathbf{p}_A = \mathbf{J}_A \Delta \mathbf{x} \tag{10}$$

In general, the number of the design variables is much greater than the number of constraints and the performance indices. Therefore, the above equation is usually underdetermined. An optimal solution to this is given by

$$\Delta \mathbf{x}^\circ = \mathbf{J}_A^\# \Delta \mathbf{p}_A \tag{11}$$

where $\mathbf{J}_A^\#$ is the pseudoinverse of $\mathbf{J}_A$. When there exists a solution to eq. (10), the solution in the above form makes the square norm $\|\Delta \mathbf{x}\|^2$ minimum. Namely, the optimal solution $\Delta \mathbf{x}^\circ$ provides the minimal changes from the original design required for achieving the goal, i.e. the specified change $\Delta \mathbf{p}_A$.

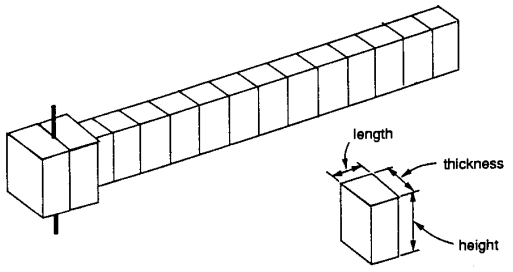

Figure 3: Finite element discretization

3.2 Computation

Using the inverse mapping method, we now determine the beam geometry that provides improved performance. Among a number of factors, the natural frequency of the fundamental mode will be of primary importance for overall control performance of the flexible arm control system. Hence, we use the lowest natural frequency as the first performance index;

$$p_1 = \omega_1 = f_1(x_1, \cdots, x_n) \tag{12}$$

As for constraints we consider the total mass M, the moment of inertia about the joint axis, I_J, and the endpoint vertical deflection for a maximum endpoint load, δ. These are all functions of the design variables $\mathbf{x}$. Namely,

$$\begin{aligned} M &= g_1(x_1, \cdots, x_n) \\ I_J &= g_2(x_1, \cdots, x_n) \\ \delta &= g_3(x_1, \cdots, x_n) \end{aligned} \tag{13}$$

As shown in Figure 3, the arm link is modeled as a series of rectangular elements. The design variables are the width and height of the individual segments, b_i and h_i.

$$\mathbf{x} = [b_1, h_1, b_2, h_2, \cdots, b_S, h_S]^T \tag{14}$$

The total length of the arm link is fixed to be $L = 0.75$ m, which is divided into $S = 22$ segments. The joint axis is also modeled as a rectangular bar, the width and height of which are assumed to be invariant and excluded in the design variables.

We begin with a given original design, which is a uniform beam having the identical cross section of 3.3 mm width and 19 mm height. As listed in Table 1, the lowest natural frequency is 22.02 Hz, whereas the total mass, moment of inertia and endpoint vertical deflection are 0.2853 kg, 0.0206 $kg \cdot m^2$, 9.72 mm, respectively.

The primary objective of modifying the arm link design is to increase the natural frequency while satisfying the other three conditions and specifications. To compute the natural frequency and the other specifications, we used an FEM package: ADINA [Bathe, 1982]. By calling the ADINA, the

Table 1: Comparision in performance indices

	Beam Mass (kg)	Inertia (kg-m^2)	End-Point Deflection(mm)	First Natural Frequency(Hz.)	Frequency (Experiment)
Nominal Design	0.2853	0.0206	9.72	22.02	19
Final Design	0.2854	0.0176	9.67	31.67	25

Table 2: Comparision in design parameters

	Nominal Design			*Final Design*		
	Length(m.)	Thickness(m.)	Width(m.)	Length(m.)	Thickness(m.)	Width(m.)
El 1	0.0125	0.025	0.1	0.0125	0.025	0.1
El 2	0.0125	0.025	0.1	0.0125	0.025	0.1
El 3	0.0355	0.0032	0.019	0.0355	0.0018	0.025
El 4	0.0355	0.0032	0.019	0.0355	0.0025	0.023
El 5	0.0355	0.0032	0.019	0.0355	0.0030	0.021
El 6	0.0355	0.0032	0.019	0.0355	0.0034	0.019
El 7	0.0355	0.0032	0.019	0.0355	0.0036	0.019
El 8	0.0355	0.0032	0.019	0.0355	0.0039	0.016
El 9	0.0355	0.0032	0.019	0.0355	0.0041	0.015
El 10	0.0355	0.0032	0.019	0.0355	0.0042	0.015
El 11	0.0355	0.0032	0.019	0.0355	0.0043	0.016
El 12	0.0355	0.0032	0.019	0.0355	0.0041	0.019
El 13	0.0355	0.0032	0.019	0.0355	0.0041	0.020
El 14	0.0355	0.0032	0.019	0.0355	0.0038	0.023
El 15	0.0355	0.0032	0.019	0.0355	0.0037	0.024
El 16	0.0355	0.0032	0.019	0.0355	0.0031	0.029
El 17	0.0355	0.0032	0.019	0.0355	0.0033	0.022
El 18	0.0355	0.0032	0.019	0.0355	0.0032	0.019
El 19	0.0355	0.0032	0.019	0.0355	0.0029	0.015
El 20	0.0355	0.0032	0.019	0.0355	0.0023	0.013
El 21	0.0355	0.0032	0.019	0.0355	0.0012	0.018
El 22	0.0355	0.0032	0.019	0.0355	0.0007	0.019

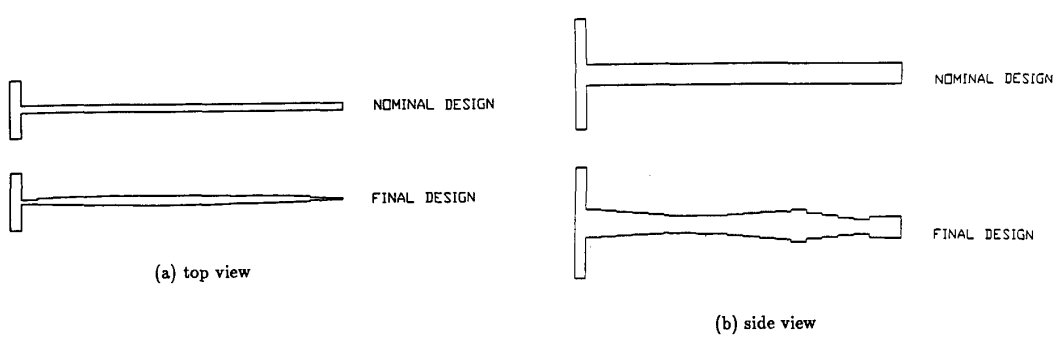

(a) top view

(b) side view

Figure 4: Comparison of the nominal and the new arms

generalized Jacobian was computed numerically. Namely, by changing each design variable x_i slightly from its nominal value, we evaluated the partial derivatives involved in the generalized Jacobian by numerical differentiation; $\Delta f_i/\Delta x_j$ and $\Delta g_i/\Delta x_j$. Computing the pseudoinverse of the Jacobian, we obtained optimal incremental changes $\Delta \mathbf{x}^\circ$ that relocate the poles in the specified direction. Next we updated the design variables so that $\mathbf{x} = \mathbf{x} + \Delta \mathbf{x}^\circ$, and then repeated the above computation until it reached a local optimum.

Table 2 and Figure 4 show the resultant link geometry derived from the iterative computations. The arm link has the same mass and the same load bearing capability, while the natural frequency increased to 31.67 *Hz*. The moment of inertia, on the other hand, reduced to 0.0176 $kg{\cdot}m^2$, which allows for higher acceleration. It is notable that the dynamic characteristics of the new beam are by far superior to the original uniform beam. The new beam has a unique profile as shown in the figure. It is thick in the middle and thinner at both ends. Usually, we imagine that the proximal section should be thicker than the distal section. Nevertheless, the beam in which the thickness decreases monotonically from the joint axis to the tip has a significantly lower natural frequency than the one shown in Figure 4. It is paradoxical that the beam with a thicker middle section provides a higher natural frequency than the one with a monotonically decreasing thickness.

4 Relocation of Zeros Using Transmission Mechanisms

The locations of poles have been improved significantly by modifying the link geometry and changing the mass and stiffness distributions. The locations of zeros can also be changed to some extent by modifying the link geometry, but its effect is limited. The zero locations are heavily dependent upon the locations of sensors and actuators, i.e. the input and output of the system. In particular, non-collocated sensors and actuators yield a non-minimum phase system, where the real positive zero might make the system unstable. Such zero locations cannot be changed by simply changing the link geometry, but the relative position between the sensor and the actuator needs to be changed. Since our ultimate goal of the arm control system is to achieve high-speed, high-accuracy endpoint positioning, the output of the system must be the position of the endpoint. In other words, the location of the sensor must be at the endpoint. In consequence, to collocate the sensor and actuator, it is necessary to locate the actuator near the endpoint, or transmit the actuator torque to an appropriate position near the endpoint, according to [Park and Asada, 1990]. In this paper we apply their torque transmission technique to the flexible arm design.

Figure 5 shows a torque transmission mechanism. Note that the drive axle of the actuator is not directly connected to the joint axis but the torque is transmitted through the transmission line to the terminal point of the transmission, called the torque application point. When the torque application point is exactly at the endpoint, the system is completely collocated. In reality, however, the torque application point does not have to be located at the endpoint but can be somewhere between the endpoint and the joint axis, because higher order zeros are not relevant to the dynamics in usual operating ranges. More detailed analysis will be shown in order to determine an optimal location for the torque application point. Anyhow, the actuator torque is applied somewhere in the middle of the arm link, where the width of the beam is thicker than that of the both ends.

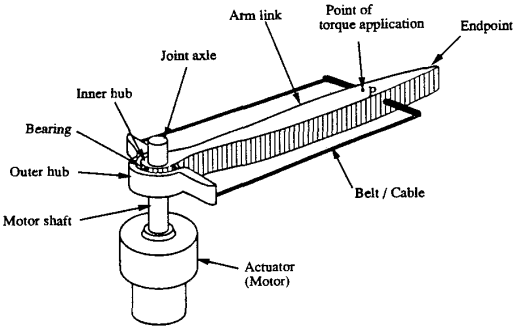

Figure 5: Single link arm with torque transmission mechanism

The zero locations can be computed by using mode functions obtained from the finite element analysis. Let $\phi_i(\zeta)$ be the i-th mode function, where ζ is the distance from the joint axis along the beam axis. Let $\zeta = c$ be the distance of the torque application point from the joint axis, and z_L the arc length of the endpoint displacement. The transfer function from the actuator torque τ to the endpoint position z_L can be obtained in the same way as in [Park and Asada, 1990].

$$G(s) = \frac{z_L(s)}{\tau(s)} = \sum_{i=0}^{N} \frac{\phi_i'(c)\phi_i(L)}{m_i(s^2+\omega_i^2)} \tag{15}$$

where coefficients m_i and ω_i are computed with the mode functions;

$$m_i = \int_0^L \rho A(\zeta)\ \phi_i^2(\zeta)\ d\zeta \tag{16}$$

$$m_i\omega_i^2 = \int_0^L EI(\zeta)\ \phi_i''^2(\zeta)\ d\zeta \tag{17}$$

Note that the cross-sectional area $A(\zeta)$ and the stiffness $EI(\zeta)$ are functions of ζ, since the beam is not uniform.

In order for the system to be of minimum phase, all the zeros of the transfer function should be in the left-half plane. Rewriting the transfer function given by eq. (15), we obtain

$$G(s) = \frac{A_N s^{2N} + A_{N-1}s^{2N-2} + \cdots + A_1 s^2 + A_0}{s^2(s^2+w_1^2)\cdots(s^2+w_N^2)} \tag{18}$$

where

$$\begin{aligned} A_N &= \sum_{i=0}^{N} \frac{\phi_i'(c)\phi_i(L)}{m_i} \\ A_{N-1} &= \sum_{i=0}^{N} \frac{\phi_i'(c)\phi_i(L)}{m_i} \sum_{j\neq i} \omega_j^2 \\ A_{N-2} &= \sum_{i=0}^{N} \frac{\phi_i'(c)\phi_i(L)}{m_i} \sum_{j,k\neq i} \omega_j^2\omega_k^2 \\ &\vdots \end{aligned}$$

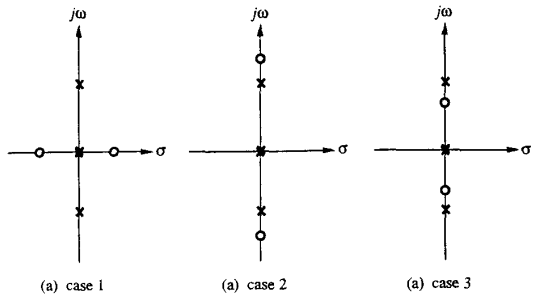

Figure 6: Configurations of pole-zero locations

$$A_0 = \sum_{i=0}^{N} \frac{\phi_i'(c)\phi_i(L)}{m_i} \prod_{j \neq i} \omega_j^2 \qquad (19)$$
$$= \frac{\phi_0'(c)\phi_0(L)}{m_0} \omega_1^2 \cdots \omega_N^2$$

From the above transfer function it follows that the dynamic characteristics vary significantly depending upon the location of torque application c. Regular flexible arms where $c = 0$ are non-minimum phase systems, as it is clear that the coefficient A_N in the numerator of eq. (18) becomes negative when $c = 0$.

As the torque application point moves toward the endpoint, the distance between the sensor and the actuator reduces. As a result, the zeros change their locations in the s-plane and the non-minimum phase zeros can be removed. In order to demonstrate this, let us consider the first two modes of the system.

$$G(s) = \frac{A_1 s^2 + A_0}{s^2(s^2 + \omega_1^2)} \qquad (20)$$

Coefficient A_1 is a function of the torque application point c, which determines the zero configuration:

Case 1 when $A_1 < 0$, the zeros are on the real axis resulting in a non-minimum phase system (Figure 6a).

Case 2 when $0 < A_1 < A_0/\omega_1^2$, the zeros are on the imaginary axis and are larger than the poles in magnitude (Figure 6b).

Case 3 when $A_1 > A_0/\omega_1^2$, the zeros are on the imaginary axis and are smaller than the poles in magnitude (Figure 6c).

5 Controller Design Integrated with Structure Design

Since conventional flexible arms are non-minimum phase systems, the phase lag is a critical issue for stability. The non-collocated sensor/actuator pair may render the closed-loop system unstable, and thus the endpoint feedback of the flexible arm may result in poor performance. In order to overcome the difficulty in control, we attempt to modify the structural part of the system. In this section, we propose an integrated approach to the structure and control design.

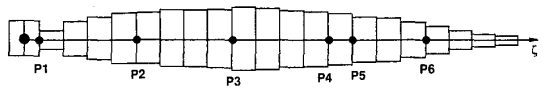

Figure 7: Arm shape (top view) and torque application points

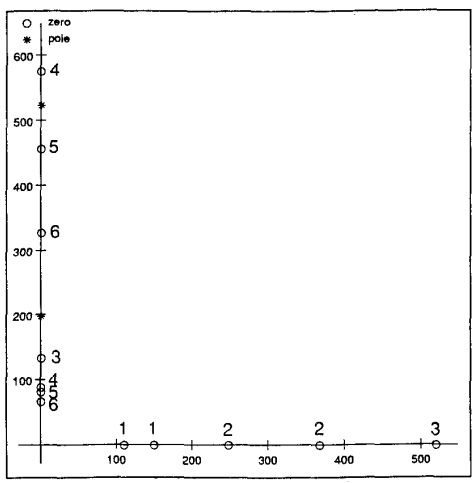

Figure 8: Pole-zero locations for varying torque application points

According to the paper by [Park and Asada, 1990], if the poles and zeros of a flexible structure are located alternatively on the imaginary axis, the system is robustified. Case 3 in the previous section meets this condition and the endpoint control system is robustly stable with a simple PD-control. When we consider up to N-th mode, the condition for the Case 3 pole-zero configuration is given by

$$c > c_{crit} \qquad (21)$$

where c_{crit} is the largest value in $0 < c < L$ that satisfies;

$$\phi_N'(c) = 0 \qquad (22)$$

Thus, the torque application point c should be located so as to satisfy eq. (21) for robustness in a given operating range.

The mode functions obtained from the finite element method are used to calculate the zeros of the system. For different torque application points as shown in Figure 7, the corresponding zeros are plotted in Figure 8 for the case of $N = 2$. Note that the figure shows only for the first quadrant of the s-plane. From the figure, we can see that there exist real zeros for actuation points P1, P2 and P3. As for point P4, all the zeros are on the imaginary axis, but one of the zeros is above the second pole, which violates the condition of Case 3. Thus, P4 is not suitable for the torque application with respect to the robustness of the system. When the

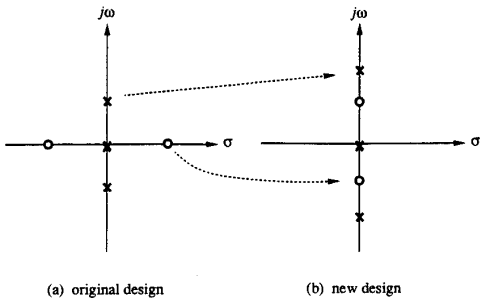

Figure 9: Transition in pole-zero locations

torque application point is further moved toward the endpoint, e.g. to P5 or P6, the zeros alternate with the poles on the imaginary axis. The critical point c_{crit} exists between P4 and P5, i.e. in the 15-th element out of 22 elements involved in the FEM model. Therefore, the location of torque application point c should be selected from the range $c > 0.65L$ when $N = 2$. If the frequency range in which the system is to be operated is low, we can neglect the second flexible mode, and the torque application point can be moved to a more proximal point, e.g. P3 and the transmission linkage can be shorter.

Next, we combine the two methods described in Sections 3 and 4; the inverse mapping for relocating the poles, and the torque transmission for relocating the zeros. To increase speed of response it is desired to locate the poles further from the origin, whereas for robust endpoint control it is desired to have the zeros on the imaginary axis closer to the origin. The open-loop, pole-zero configuration of the original flexible arm is shown in Figure 9-a, where the zeros are on the real axis. The corresponding figure for the new design (Figure 9-b) shows that the zeros have moved onto the imaginary axis and that the poles have moved further from the origin.

In the resultant design, the link geometry was optimized for increasing the natural frequency, which resulted in a thin section near the joint axis. If the actuator torque is directly applied to the joint, the thin beam section near the joint axis may yield a large deflection. In the proposed design, the actuator torque is by-passed to the thick section in the middle. As a result, the beam deflection is much smaller than that of the direct torque application to the joint axis. In this design, we modified the pole location by changing the link geometry, and the zero location by the torque transmission line. Both the poles and zeros are relocated to the desired positions separately, but these two are fortunately non-conflicting requirements to each other.

6 Implementation and Experiments

In order to verify the improvements of the new arm, a prototype flexible arm was built based on the numerical data given in Table 2. Due to difficulties in machining, the beam profile was simplified. For comparison, the original arm with a uniform cross section was also built and tested at the same time.

First, an open-loop test was conducted to evaluate the increase of the first natural frequency. We applied external disturbances by hitting the arm in the middle, then the frequency of vibration was measured. As listed in Table 1, the first natural frequency increased from 19 *Hz* to 25 *Hz* in the new design. Thus, by reshaping the arm profile, the natural frequency was significantly increased.

7 Conclusion

The integrated structure/control design of flexible robot arms has been presented. The open-loop, poles and zeros are relocated by modifying the geometry and the structure of the arm. To determine the geometry and structure in a systematic manner, an inverse mapping method based on finite element modeling and sensitivity analysis has been developed and applied to the flexible arm design. Using this method, a unique beam geometry that allows for a significantly high natural frequency has been obtained. In order to relocate zeros, we have applied the torque transmission technique that allows us to remove non-minimum phase zeros and make the endpoint control robustly stable. Based on the theoretical analysis and computation, a prototype arm was designed and built, and its performance was evaluated.

References

Baillieul, J., (1986), "Avoiding Obstacles and Resolving Kinematic Redundancy," *Proc. 1986 IEEE Int. Conf. Robotics and Automation,* pp.1698-1707.

Bathe, K.-J., (1982), *Finite Element Procedures in Engineering Analysis*, Prentice-Hall, New Jersey.

Belvin, W. K. and Park, K. C., (1990), "Structural Tailoring and Feedback Control Synthesis: An Interdisciplinary Approach," *J. of Guidance, Control, and Dynamics,* Vol.13, No.3, pp.424-429.

Kosut, R. L., Kabuli, G. M., Morrison, S., and Harn, Y.-P., (1990), "Simultaneous Control and Structure Design for Large Space Structures ," *Proc. 1990 American Control Conference,* pp.860-865.

Lim, K. B. and Junkins, J. L., (1989), "Robust Optimization of Structural and Controller Parameters," *J. of Guidance, Control, and Dynamics,* Vol.12, No.1, pp.89-96.

Park, J.-H. and Asada, H., (1990), "Design and Control of Minimum Phase Flexible Arms with Torque Transmission Mechanisms," *Proc. 1990 IEEE Int. Conf. on Robotics and Automation,* pp.1790-1795.